

CERIAS Tech Report 2007-72

Channel Model and Operational Capacity Analysis of Printed Text Documents

by A. K. Mikkilineni, P.-J. Chiang, G. T.-C. Chiu, J. P. Allebach, E. J. Delp

Center for Education and Research

Information Assurance and Security

Purdue University, West Lafayette, IN 47907-2086

Channel Model and Operational Capacity Analysis of Printed Text Documents

Aravind K. Mikkilineni[‡], Pei-Ju Chiang[‡]
George T. C. Chiu[‡], Jan P. Allebach[†], Edward J. Delp[†]

[†]School of Electrical and Computer Engineering

[‡]School of Mechanical Engineering

Purdue University, West Lafayette, Indiana USA

ABSTRACT

In today's digital world securing different forms of content is very important in terms of protecting copyright and verifying authenticity. One example is watermarking of digital audio and images. We believe that a marking scheme analogous to digital watermarking but for documents is very important. In this paper we describe the use of laser amplitude modulation in electrophotographic printers to embed information in a text document. In particular we describe an embedding and detection process which allows the embedding of between 2 and 8 bits in a single line of text. For a typical 12 point document this translates to between 100 and 400 bits per page. We also perform an operational analysis to compare two decoding methods using different embedding densities.

Keywords: document security, secure printing, printer identification

1. INTRODUCTION

In today's digital world securing different forms of content is very important in terms of protecting copyright and verifying authenticity[1–10]. One example is watermarking of digital audio and images. We believe that a marking scheme analogous to digital watermarking but for documents is very important[1]. Printed material is a direct accessory to many criminal and terrorist acts. Examples include forgery or alteration of documents used for purposes of identity, security, or recording transactions. In addition, printed material may be used in the course of conducting illicit or terrorist activities. Examples include instruction manuals, team rosters, meeting notes, and correspondence. In both cases, the ability to identify the device or type of device used to print the material in question would provide a valuable aid for law enforcement and intelligence agencies. We also believe that average users need to be able to print secure documents, for example boarding passes and bank transactions.

There currently exist techniques to secure documents such as bank notes using paper watermarks, security fibers, holograms, or special inks[11, 12]. The problem is that the use of these security techniques can be cost prohibitive. Most of these techniques either require special equipment to embed the security features, or are simply too expensive for an average consumer. Additionally, there are a number of applications in which it is desirable to be able to identify the technology, manufacturer, model, or even specific unit that was used to print a given document.

We propose to develop two strategies for printer identification based on examining a printed document. The first strategy is passive. It involves characterizing the printer by finding intrinsic features in the printed document that are characteristic of that particular printer, model, or manufacturer's products. We refer to this as the *intrinsic signature*. The intrinsic signature requires an understanding and modeling of the printer mechanism, and the development of analysis tools for the detection of the signature in a printed page with arbitrary content.

We have previously reported techniques that use the print quality defect known as *banding* in electrophotographic (EP) printers as an intrinsic signature to identify the model and manufacturer of the printer[13–15]. We showed that different printers have different sets of *banding frequencies* which are dependent upon brand and

This research was supported by a grant from the National Science Foundation, under Award Number 0524540. Address all correspondence to E. J. Delp at ace@ecn.purdue.edu

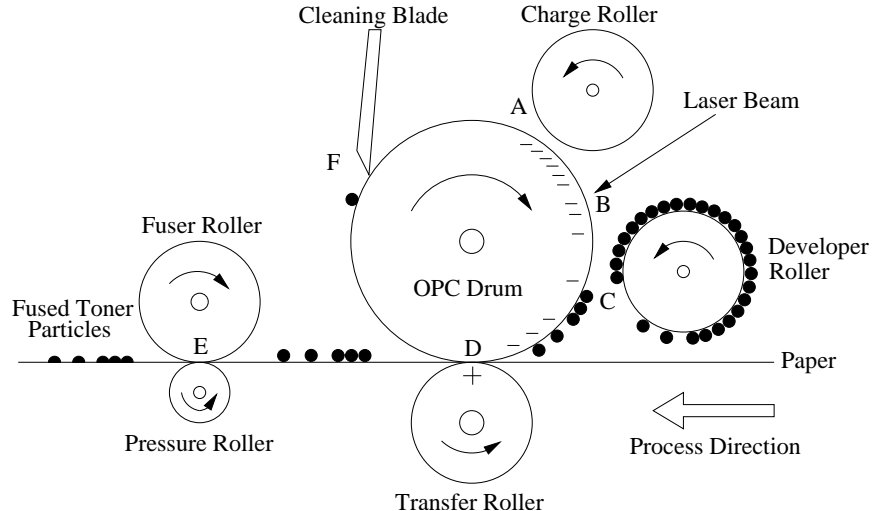


Figure 1. Diagram of the EP process: (A) charging, (B) exposure, (C) development, (D) transfer, (E) fusing, (F) cleaning

model. By using texture features to characterize this intrinsic signature, we have been able to correctly identify the source printer of printed text documents generated by both EP and inkjet printers[16–19].

The second strategy is active. We embed an *extrinsic signature* in a printed page. This signature is generated by modulating the process parameters in the printer mechanism to encode identifying information such as the printer serial number and date of printing. To detect the extrinsic signature we use the tools developed for intrinsic signature detection. We have successfully been able to embed information into a document with electrophotographic (EP) printers by modulating the banding intrinsic feature[20].

Embedding extrinsic features into a document also requires knowledge of the specific print mechanism. During the past few years, many techniques to reduce banding artifacts have been successfully demonstrated by modulating various process parameters such as laser intensity/timing/pulse width (exposure modulation)[21], motor control[22], and laser beam steering[23]. These techniques can also be used to inject “artificial” banding signals that are not intrinsic to the printer. The technological understanding and capability to implement these techniques are not easily obtained meaning it will be difficult for someone to “hack” it.

One issue with embedding extrinsic signatures is that the information should not be detectable by the human observer but needs to be detectable by suitable detection algorithms.[20] This can be accomplished by exploiting the band-pass characteristics of the human visual system with regard to contrast sensitivity. An HP Color LaserJet 4500 is used as the experimental platform for this study. Although a print color engine is used as the experimental system, we will focus only on the monochrome results for this study.

Previously we have demonstrated this ability to embed an extrinsic signature in documents which contain halftone images or text[20, 24–27]. Using a frequency shift keying modulation scheme[27], we were able to embed 150 bits into a full page of 12 point text, or 3 bits in each text line.

In the following sections we will extend our current work on modeling of the text document as a communication channel. Additional embedding methods will be explored to enable embedding of up to 400 bits in a page of 12 point text. Also the performance of two different decoding methods will be compared.

2. EP EMBEDDING TECHNIQUES

Figure 1 shows a side view of a typical EP printer. The print process has six steps. The first step is to uniformly charge the optical photoconductor (OPC) drum. Next a laser scans the drum and discharges specific locations on the drum. This is the “exposure” step. The discharged locations on the drum attract toner particles which are then attracted to the paper which has an opposite charge. Next the paper with the toner particles on it

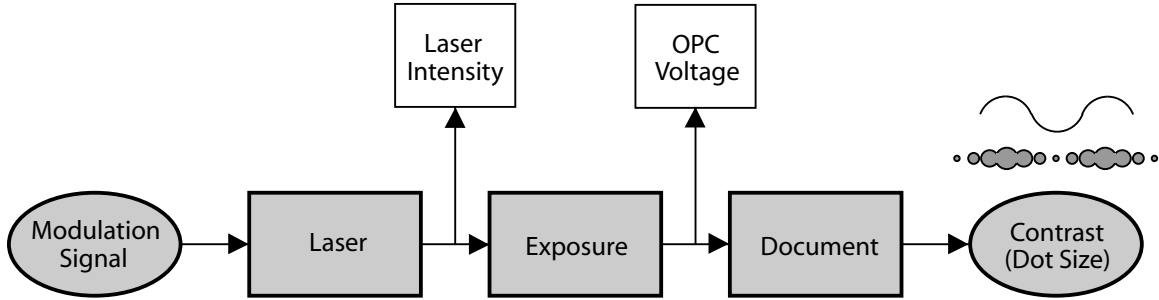


Figure 2. Process block diagram for embedding extrinsic banding signature using laser intensity modulation

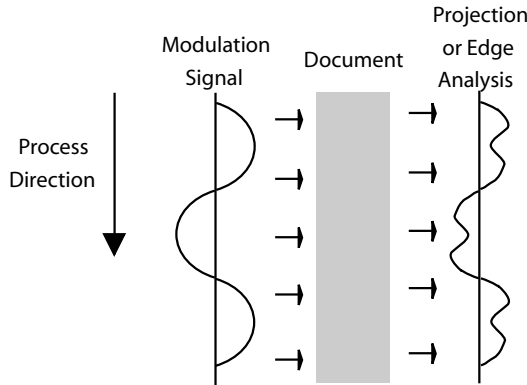


Figure 3. Embedding and detecting extrinsic banding signal

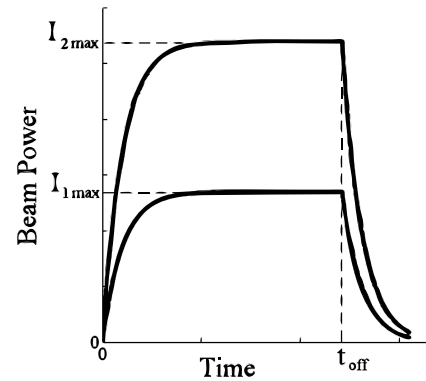


Figure 4. Laser power profile

passes through a fuser and pressure roller which melts and permanently affixes the toner to the paper. Finally a blade or brush cleans any excess toner from the OPC drum.

In EP printing, artifacts are created in the printed output due to electromechanical imperfections in the printer such as fluctuations in the angular velocity of the OPC drum, gear eccentricity, gear backlash, and polygon mirror wobble. In previous work we have shown that these imperfections are directly related to the electromechanical properties of the printer. This property allows the corresponding fluctuations in the developed toner on the printed page to be treated as an intrinsic signature of the printer.

The most visible print quality defect in the EP process is banding, which appears as cyclic light and dark bands most visible in midtone regions of the document. Many banding reduction techniques have been successfully demonstrated. These techniques, three of which are laser intensity/timing/pulse width[21], motor control[22], and laser beam steering[23], actively modulate certain process parameters.

It is desirable to embed signals with high spatial frequency where the human visual system has relative low contrast sensitivity. Among the methods mentioned above, motor control has difficulty controlling the EP process at high spatial frequencies due to inherent electro-mechanical limitations. Laser beam steering requires additional process capability that is not found in typical EP engines. However, modulating various laser parameters to affect exposure, such as laser power, is common practice in typical EP process controls.

As we have shown in[20], these techniques can be used to inject an “artificial” banding signal into the document. In particular, we developed a system shown in Figure 2 using laser intensity modulation which allows per-scan-line changes in laser intensity.

2.1. Relationship Between Laser Power and Exposure

During the EP printing process, the image to appear on paper is first written onto an OPC drum by a laser. The intensity profile of the laser beam is modeled as a 2-D Gaussian envelope[28, 29], which is given by

$$I(x, y, t) = I_0(t) \exp\left(-\frac{y^2}{2\alpha^2} - \frac{x^2}{2\beta^2}\right) \frac{W}{m^2} \quad (1)$$

where $I_0(t)$ represents the laser power, and α and β are the standard deviations of the laser beam profile in the process y and scan x directions respectively. Assume the laser is switched on at time $t = 0$ and off at time $t = t_{off}$ and the rise and fall transition are modeled as an exponential function, see Figure 4. Then the laser power can be expressed as

$$I_0(t) = \begin{cases} 0 & , \quad t < 0 \\ I_{max}(1 - e^{-\frac{t}{t_r}}) & , \quad 0 \leq t \leq t_{off} \\ I_{max}(1 - e^{-\frac{t_{off}}{t_r}})e^{-\frac{(t-t_{off})}{t_f}} & , \quad t > t_{off} \end{cases} \quad (2)$$

where I_{max} is the maximum allowable laser power. This parameter, I_{max} , is directly related to and controlled by a voltage V_{ref} on the driver chip of the laser and is not shown in the equations.

Let the nominal values of the printed pixel width in the scan direction and process direction be X and Y , respectively. Assume the laser beam translates along the scan direction x at a velocity V which is extremely high compared with the motion of the photoconductor surface. Then the exposure energy at any arbitrary point (x, y) due to the pixel $[m, n]$ being turned on is found by integrating Equation 2 with respect to time.

$$E_{mn}(x, y) = \int I_0(t) \exp\left(-\frac{(y - y_n)^2}{2\alpha^2} - \frac{(x - (x_m - \frac{X}{2}) - Vt)^2}{2\beta^2}\right) dt \quad \frac{J}{m^2} \quad (3)$$

Since the exposure of each printed pixel is additive, the overall exposure at any given point on the OPC is the sum of exposures contributed from each neighboring pixel.

$$E(x, y) = \sum_{m,n} E_{mn}(x, y) \quad (4)$$

The exposure can be controlled by adjusting I_{max} (amplitude modulation), or adjusting the duration of the laser pulses (pulse width modulation or PWM)[21]. Both methods control $I_0(t)$, the laser power. In this study, we used amplitude modulation to control exposure. As shown in Figure 4, when I_{max} is increased, the laser power $I_0(t)$ and the total exposure energy are also increased.

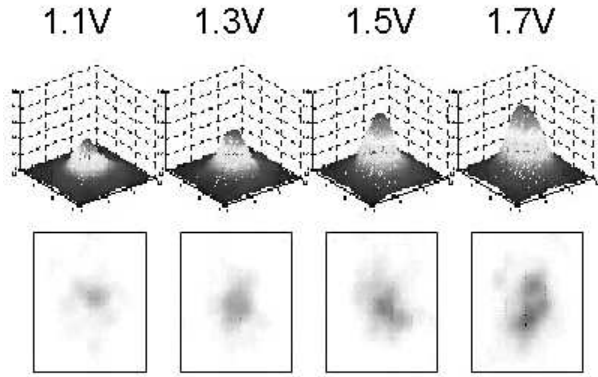
After the photoconductor is exposed by the laser beam, a latent image is produced on the photoconductor surface. Charged toner particles are attracted to the latent image and then transferred and fused to the paper. Based on the discharged electric potential, the tone value adhered on the photoconductor can be estimated. Here the photoconductor surface voltage after exposure, the light voltage V_L [28], can be written as

$$V_L = V_{sat} + (V_D - V_{sat}) \exp\left(-\frac{E}{E_a}\right) \quad Volts \quad (5)$$

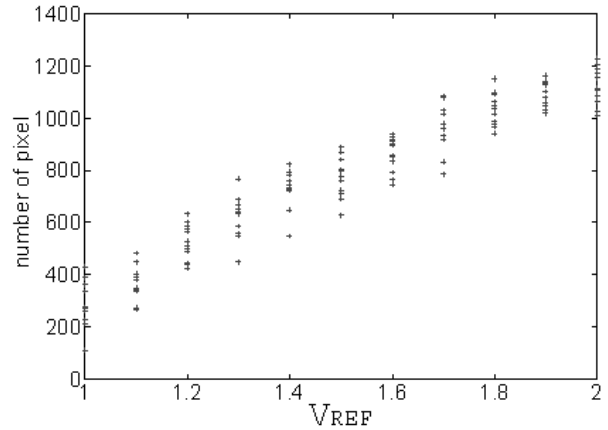
where V_{sat} is the voltage obtained for very high exposure energy, V_D is the dark voltage, E is the exposure energy, and E_a is the energy constant that describes the sensitivity of the photoconductor. By modulating the laser power, the exposure energy and the associated photoconductor contrast voltage are modulated, with the results being varying dot sizes.

As mentioned earlier in this section, modulation of the laser power is performed through modulation of the voltage V_{ref} . For our test printer, the nominal value for V_{ref} is 1.5V. The allowable range for V_{ref} is from 1.0V to 2.0V.

Figure 5(a) shows the average dot profile of 16 dots when V_{ref} is held constant at 1.1, 1.3, 1.5 and 1.7 volts. Figure 5(b) shows the relationship between the input voltage and dot size. The dot size is determined by counting the number of pixels with absorptance greater than 0.1 in one dot cell. As the input voltage increases, the dot size increases. However, as seen in Figure 5(b), instabilities in the EP process cause variations in the dot sizes developed on the paper. This behaviour can create the potential for ambiguity if the chosen detection technique relies heavily on particular embedding levels or dot sizes.



(a) Dot profiles for different V_{ref}



(b) Dot size versus V_{ref}

Figure 5. Effect of V_{ref} on dot size

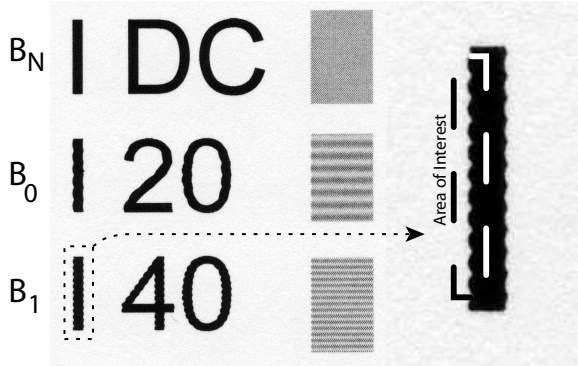


Figure 6. Large amplitude exposure modulation. 1st line no modulation, 2nd line 20 cycles/in, 3rd line 40 cycles/in

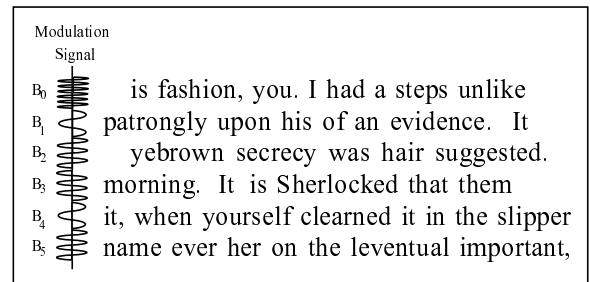


Figure 7. Modulation scheme for text documents

2.2. The Effects of Laser Intensity Modulation

Figure 6 shows the effect of modulating laser intensity in different types of images. The first line is printed without any modulation. The second line is modulated with a high power 20 cycle/inch sinusoidal signal. The third line is modulated with a high power 40 cycle/inch sinusoidal signal. These signals can be easily seen in the halftone patches of Figure 6. This is because the frequency/amplitude combination of the signals are above the threshold developed in[30] below which human perceptibility is low.

However, this same signal is not perceptible in the saturated interior region of the text characters of Figure 6. This is not true for the edges of the text characters, specifically the left and right edges where the existence of the embedded signal is clearly seen in the enlarged character 'I' from the third line. This behavior allows the embedded signal to be estimated through extraction and analysis of the edges of individual text characters as described in[24].

3. EMBEDDING AND DETECTION

A channel model of a printed text document is necessary for understanding the capacity limits and embedding techniques that can be used for embedding extrinsic information into a document. One approach is to model each individual text line as a signaling period during which one channel symbol is sent. At the decoder side, the

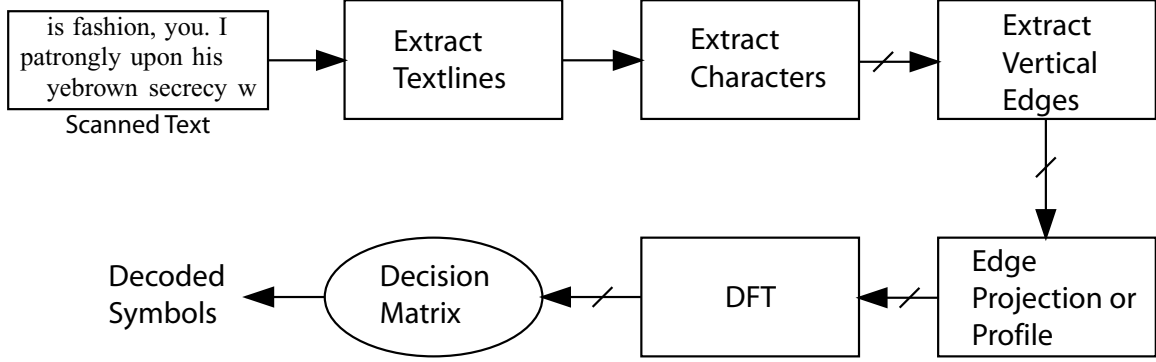


Figure 8. Process for extracting embedded information

fact that each individual character contains a version of the same channel symbol can be viewed as a form of receiver diversity.

Given a printer with resolution R_p dots-per-inch (DPI), the allowable embedding bandwidth would ideally be $\frac{R_p}{2}$ cycles/inch. However, the allowable bandwidth drops significantly after taking into account the printer MTF[25]. Furthermore, the signaling period length determines the frequency resolution at the decoder. For a font size f_s , the maximum signaling period length is $L_{max} = \frac{f_s}{72}R_s$ where R_s is the scan resolution. The smallest resolvable frequency separation is then $\frac{R_s}{L_{max}}$. For 12 point text this means $L_{max} = 400$ which gives between 6 and 18 cycle/inch separation for uppercase and lowercase characters respectively for a 2400 DPI scan. Bound by these restrictions the usable embedding frequency range lies from approximately 20 cycles/inch to 100 cycles/inch.

In[27] a signal set was considered consisting of 9 individual sinusoidal signals of the form

$$x_i(y) = \sin\left(\frac{2\pi f_i y}{R_s}\right), \quad (6)$$

where $f_i \in \{20, 30, 40, \dots, 100\}$. Each signal corresponds to one symbol which is embedded into a text line as shown in Figure 7. This scheme allows approximately 3 bits of information to be embedded into each text line. The use of phase information was also proposed to increase the number of usable symbols, however estimation of the signal phase has proved to be difficult.

As an alternative to adding phase information, the signals can be defined as follows. Let $\mathbf{b} = \{b_0, b_1, \dots, b_n\}$ be a set of bits to be embedded into a line of text. The corresponding signal $B(y)$ can then be defined as

$$B(y) = \sum_{i=0}^n b_i A_i \sin\left(\frac{2\pi f_i y}{R_p}\right), \quad (7)$$

where

$$\mathbf{f} = f_0, f_1, \dots, f_n, \quad (8)$$

$$A_i = \frac{n-i}{n} A_{max} + \frac{i}{n} A_{min}. \quad (9)$$

A_{max} is the amplitude to be used for frequency f_0 and A_{min} is the amplitude to be used for frequency f_n . The amplitude varies linearly between these two values for frequencies between f_0 and f_n . This new signal $B(y)$ is a sum of sinusoids. When viewed in the frequency domain, each frequency f_i corresponds to one bit in \mathbf{b} . For example, if $n = 8$, there would be 256 symbols, each corresponding to a different \mathbf{b} .

The decoding process to extract and decode the embedded signals $B(y)$ is outlined in Figure 8. First the document is scanned at a resolution $R_s = 2400$. Individual lines of text are then extracted and processed individually in the following blocks to determine what symbol was embedded in it.

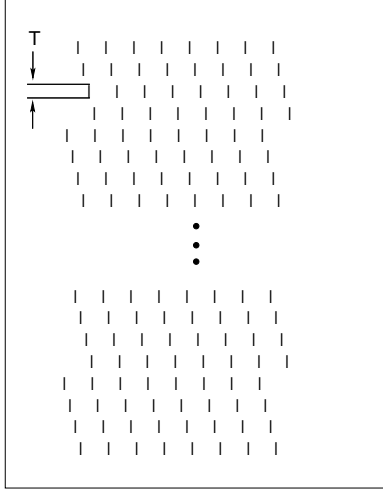


Figure 9. Test document

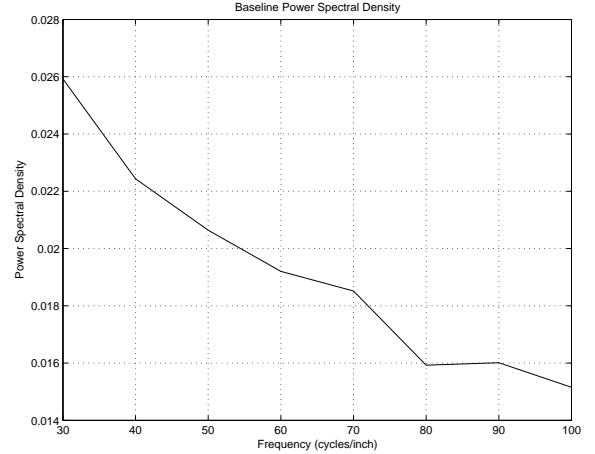


Figure 10. Baseline PSD from 432 characters

All characters in the line of text are segmented from the scanned image using techniques developed in[13]. Each character is then filtered using a threshold edge detector and morphological operations to find all the left edges of the characters. Only vertical edges that are long enough to contain at least one cycle of the lowest possible embedding frequency are used for decoding.

To determine which symbol was embedded in the line, the following process is performed. First the edge profile $\hat{B}[y]$ is found for each extracted edge from the line. The power spectral density (PSD) of each profile is obtained using a 240 point DFT as shown in Equation 10. 240 points are used to create 10 cycle/inch wide bins centered at the frequencies of interest.

$$S_{\hat{B}}[k] = \left(\sum_{n=0}^{239} \hat{B}[n] e^{j \frac{2\pi * k * n}{240}} \right)^2 \quad (10)$$

The original embedding frequencies are chosen as those with PSD values greater than some threshold determined by empirical measurements or observations.

4. RESULTS

Eight bit symbols are used with $\mathbf{f} = \{30, 40, 50, 60, 70, 80, 90, 100\}$ for the initial experiments. The symbols are embedded one per line into a test document shown in Figure 9. This test document consists of 12 point height vertical lines meant to represent the left edges of characters such as 'l', 'I', 'M', 'N', and 'b'. The page is printed on an HP Color LaserJet 4500, which is a 600 DPI printer. The printed page is then scanned using an Epson Perfection 4490 flatbed scanner at 2400 DPI in 16 bit grayscale mode with no exposure correction.

Figure 10 shows the baseline average PSD from lines with no signals embedded in them. Since the standard deviation is negligible, on the order of 10^{-4} , it might seem reasonable to define the decision thresholds near the baseline average. However, spectral leakage due to windowing artifacts and signal design will raise this threshold when multiple signals are embedded.

Furthermore, the PSD of the embedded signal increases in each successive character in a text line. Figure 11 shows the PSD for the last character in a text line embedded with symbol 80, or $\mathbf{b} = \{01010000\}$. Figure 12 shows the PSDs from 10 characters in the same line. The PSD increases monotonically starting from the leftmost character in the line. The cause of this behavior is currently unknown, although it is suspected that non-uniform charge/discharge characteristics of the OPC drum may be part of the cause. Empirical measurements of the PSDs of the last character in each line lead us to set our decision threshold at 0.10.

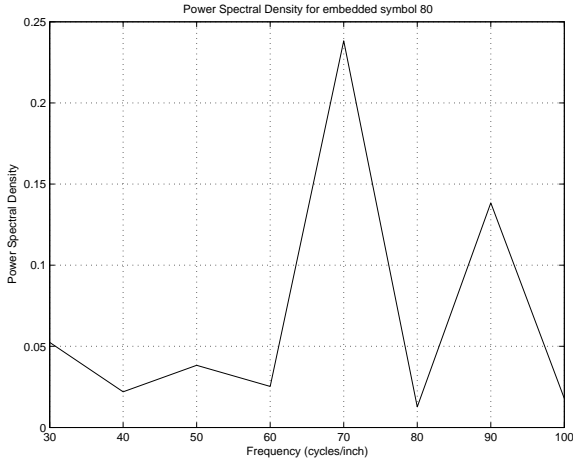


Figure 11. PSD of last character in text line with $\mathbf{b} = \{01010000\}$

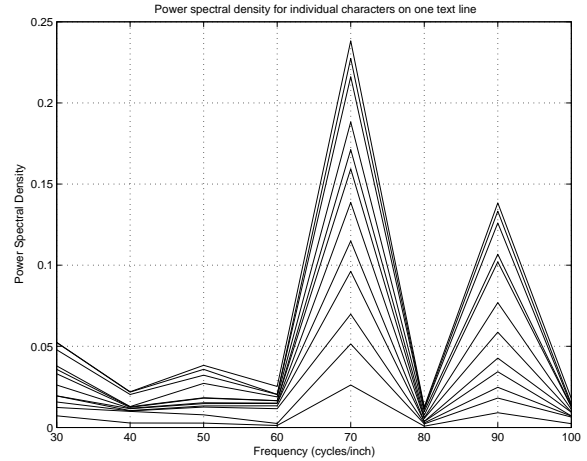


Figure 12. PSDs of 10 characters in text line with $\mathbf{b} = \{01010000\}$

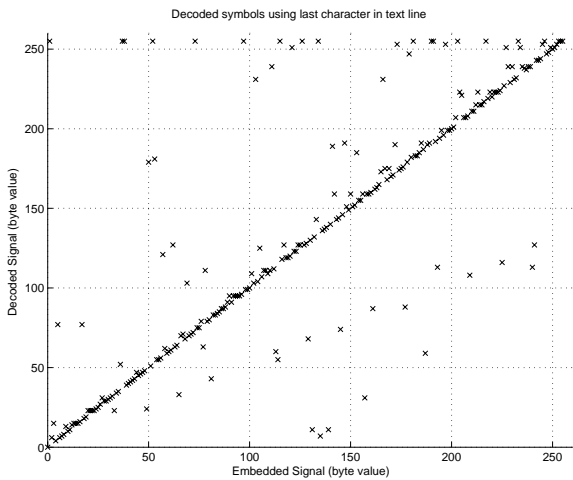


Figure 13. Decoded symbols using only last character in text line

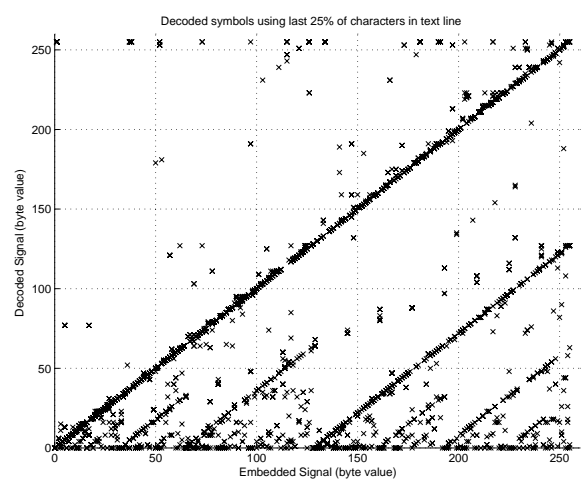


Figure 14. Decoded symbols using last 25% of characters in text line

Figures 13-16 show the decoding results using the empirically derived decision threshold. Figure 13 shows the decoding results using all 8 bits and only the last character in the text line. Figure 14 implies that there are many single bit errors. The decoding performance is slightly better using only the 6 highest frequencies in the symbols embedded as seen in Figures 15 and 16. Using a better threshold decision process should remove these errors.

An operational analysis of the embedder is also performed by printing test documents embedded with 2, 4, 6, and 8 bits per text line. Each document is decoded and the percentage error at the symbol and bit level obtained. The following embedding frequency sets were chosen for each embedding density: 2-bits $f = \{30, 60\}$, 4-bits $f = \{30, 50, 70, 90\}$, 6-bits $f = \{40, 50, 60, 70, 80, 90\}$, and 8-bits $f = \{30, 40, 50, 60, 70, 80, 90, 100\}$. Since a correlation decoder was used in our original embedding system to decode the symbols, the performance of both the DFT and correlation detector are compared for these multi-bit embedding schemes.

Figures 17 and 18 show the percentage of correctly decoded symbols using the DFT and correlation decoder respectively, for symbol sizes of 2, 4, 6, and 8 bits. The DFT detector outperforms the correlation decoder on all embedding densities. The same is seen in Figures 19 and 20 where the bit decoding errors are plotted for both the DFT and correlation decoder respectively.

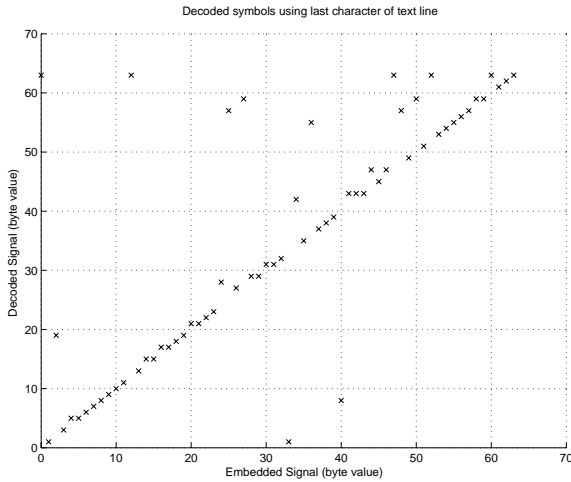


Figure 15. Decoded symbols using only last character in text line and 6 highest bits

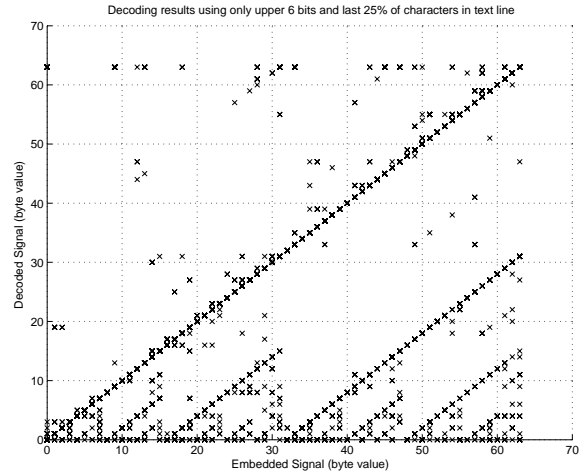


Figure 16. Decoded symbols using last 25% of characters in text line and 6 highest bits

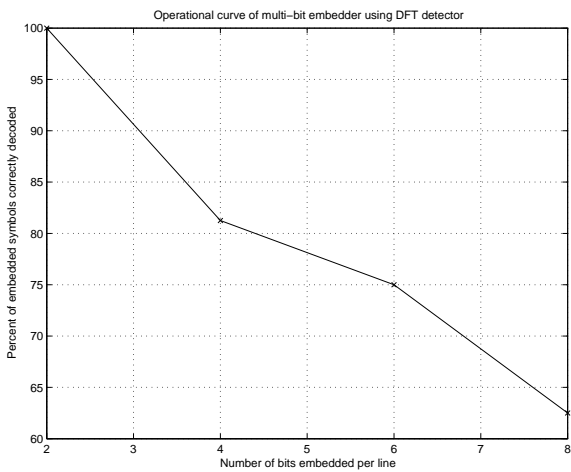


Figure 17. Symbol level operational curve using DFT decoder

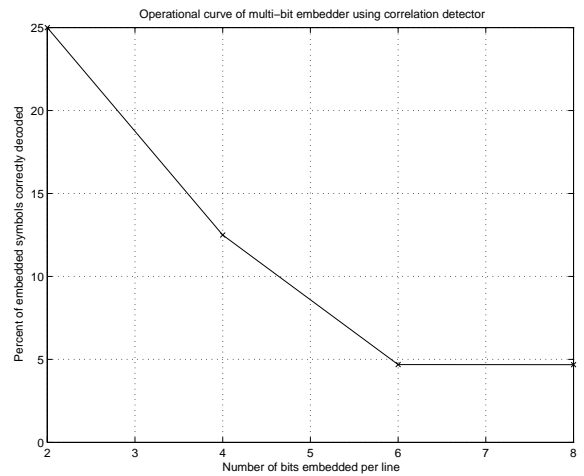


Figure 18. Symbol level operational curve using correlation decoder

5. CONCLUSIONS

As embedding density increases, the importance of a good decoding method becomes more important. In the operational curves shown in Figures 17- 20, the DFT decoder is shown to perform much better than the correlation detector even though the performance of the DFT decoder drops as the embedding density increases.

The drop in DFT decoder performance can be compensated partly by better choice of thresholds for deciding when a bit was embedded. Since it is known that spectral leakage will occur due to the inherent windowing and the signal choice itself, the power or threshold for each spectral band can be adjusted based on an initial estimate of the embedded frequencies. The thresholds can further be adjusted based on the position of the character in the text line.

REFERENCES

1. E. J. Delp, "Is your document safe: An overview of document and print security," *Proceedings of the IS&T International Conference on Non-Impact Printing*, San Diego, California, September 2002.

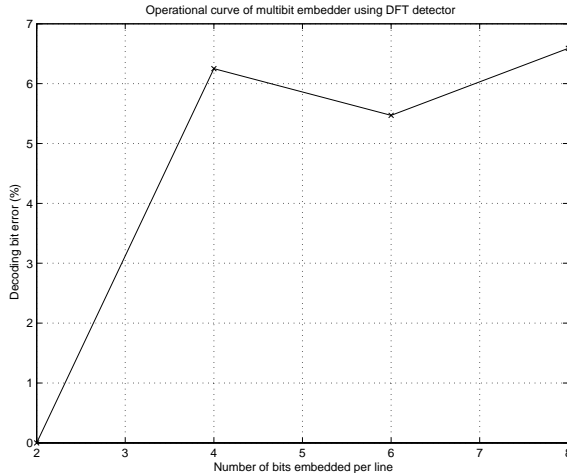


Figure 19. Bit level operational curve using DFT decoder

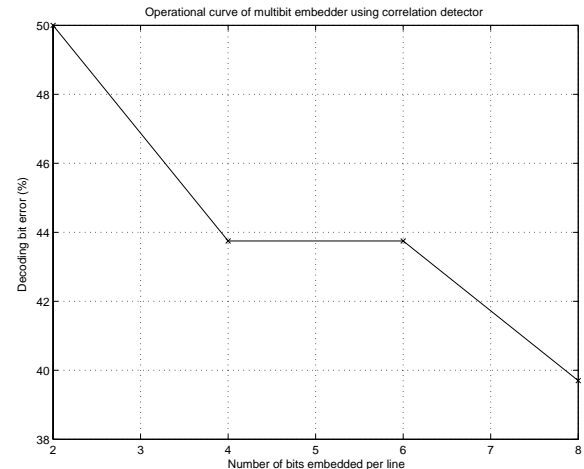


Figure 20. Bit level operational curve using correlation decoder

2. A. M. Eskicioglu and E. J. Delp, "An overview of multimedia content protection in consumer electronics devices," *Signal Processing : Image Communication*, vol. 16, pp. 681–699, 2001.
3. A. M. Eskicioglu, J. Town, and E. J. Delp, "Security of digital entertainment content from creation to consumption," *Signal Processing : Image Communication*, vol. 18, no. 4, pp. 237–262, April 2003.
4. C. I. Podilchuk and E. J. Delp, "Digital watermarking: Algorithms and applications," *IEEE Signal Processing Magazine*, vol. 18, no. 4, pp. 33–46, July 2001.
5. M. Barni, C. I. Podilchuk, F. Bartolini, and E. J. Delp, "Watermark embedding: hiding a signal within a cover image," *IEEE Communications Magazine*, vol. 39, no. 8, pp. 102–108, August 2001.
6. B. Macq, J. Dittmann, and E. J. Delp, "Benchmarking of image watermarking algorithms for digital rights management," *Proceedings of the IEEE*, 2004, to appear in.
7. R. W. Wolfgang, C. I. Podilchuk, and E. J. Delp, "Perceptual watermarks for digital images and video," *Proceedings of the IEEE*, vol. 87, no. 7, July 1999, pp. 1108–1126.
8. N. Khanna, A. Mikkilineni, A. Martone, G. Ali, G. Chiu, J. Allebach, and E. Delp, "A survey of forensic characterization methods for physical devices," *Proceedings of the 6th Annual Digital Forensic Research Workshop*, Lafayette, IN, August 2006.
9. A. F. Martone, A. K. Mikkilineni, and E. J. Delp, "Forensics of things," *Proceedings of the 2006 IEEE Southwest Symposium on Image Analysis and Interpretation*, Denver, Colorado, March 2006, pp. 149–152.
10. E. T. Lin, A. M. Eskicioglu, R. L. Lagendijk, and E. J. Delp, "Advances in digital video content protection," *Proceedings of the IEEE*, vol. 1, pp. 234–257, January 2005.
11. R. L. van Renesse, "Paper based document security - a review," *IEE European Conference on Security and Detection*, no. 437, pp. 75–80, April 1997.
12. R. L. Renesse, *Optical Document Security*. Boston: Artech House, 1998.
13. A. K. Mikkilineni, G. N. Ali, P.-J. Chiang, G. T. Chiu, J. P. Allebach, and E. J. Delp, "Signature-embedding in printed documents for security and forensic applications," *Proceedings of the SPIE International Conference on Security, Steganography, and Watermarking of Multimedia Contents VI*, vol. 5306, San Jose, CA, January 2004, pp. 455–466.
14. G. N. Ali, P.-J. Chiang, A. K. Mikkilineni, J. P. Allebach, G. T. Chiu, and E. J. Delp, "Intrinsic and extrinsic signatures for information hiding and secure printing with electrophotographic devices," *Proceedings of the IS&T's NIP19: International Conference on Digital Printing Technologies*, vol. 19, New Orleans, LA, September 2003, pp. 511–515.

15. G. N. Ali, P.-J. Chiang, A. K. Mikkilineni, G. T.-C. Chiu, E. J. Delp, and J. P. Allebach, "Application of principal components analysis and gaussian mixture models to printer identification," *Proceedings of the IS&T's NIP20: International Conference on Digital Printing Technologies*, vol. 20, Salt Lake City, UT, October/November 2004, pp. 301–305.
16. A. K. Mikkilineni, P.-J. Chiang, G. N. Ali, G. T.-C. Chiu, J. P. Allebach, and E. J. Delp, "Printer identification based on textural features," *Proceedings of the IS&T's NIP20: International Conference on Digital Printing Technologies*, vol. 20, Salt Lake City, UT, October/November 2004, pp. 306–311.
17. A. K. Mikkilineni, P.-J. Chiang, G. N. Ali, G. T. C. Chiu, J. P. Allebach, and E. J. Delp, "Printer identification based on graylevel co-occurrence features for security and forensic applications," *Proceedings of the SPIE International Conference on Security, Steganography, and Watermarking of Multimedia Contents VII*, vol. 5681, San Jose, CA, March 2005, pp. 430–440.
18. A. K. Mikkilineni, O. Arslan, P.-J. Chiang, R. M. Kumontoy, J. P. Allebach, G. T.-C. Chiu, and E. J. Delp, "Printer forensics using svm techniques," *Proceedings of the IS&T's NIP21: International Conference on Digital Printing Technologies*, vol. 21, Baltimore, MD, October 2005, pp. 223–226.
19. O. Arslan, R. M. Kumontoy, P.-J. Chiang, A. K. Mikkilineni, J. P. Allebach, G. T. C. Chiu, and E. J. Delp, "Identification of inkjet printers for forensic applications," *Proceedings of the IS&T's NIP21: International Conference on Digital Printing Technologies*, vol. 21, Baltimore, MD, October 2005, pp. 235–238.
20. P.-J. Chiang, G. N. Ali, A. K. Mikkilineni, G. T.-C. Chiu, J. P. Allebach, and E. J. Delp, "Extrinsic signatures embedding using exposure modulation for information hiding and secure printing in electrophotographic devices," *Proceedings of the IS&T's NIP20: International Conference on Digital Printing Technologies*, vol. 20, Salt Lake City, UT, October/November 2004, pp. 295–300.
21. G.-Y. Lin, J. M. Grice, J. P. Allebach, G. T.-C. Chiu, W. Bradburn, and J. Weaver, "Banding artifact reduction in electrophotographic printers by using pulse width modulation," *Journal of Imaging Science and Technology*, vol. 46, no. 4, pp. 326–337, July/August 2002.
22. C.-L. Chen, G. T.-C. Chiu, and J. P. Allebach, "Banding reduction in electrophotographic processes using human contrast sensitivity function shaped photoconductor velocity control," *The Journal of Imaging Science and Technology*, vol. 47, no. 3, pp. 209–223, May/June 2003.
23. M. T. S. Ewe, G. T.-C. Chiu, J. M. Grice, J. P. Allebach, C. Chan, and W. Foote, "Banding reduction in electrophotographic processes using a piezoelectric actuated laser beam deflection device," *The Journal of Imaging Science and Technology*, vol. 46, no. 5, pp. 433–442, September/October 2002.
24. A. K. Mikkilineni, P.-J. Chiang, S. Suh, G. T.-C. Chiu, J. P. Allebach, and E. J. Delp, "Information embedding and extraction for electrophotographic printing processes," *Proceedings of the SPIE International Conference on Security, Steganography, and Watermarking of Multimedia Contents VIII*, vol. 6072, San Jose, CA, January 2006.
25. P.-J. Chiang, A. K. Mikkilineni, E. J. Delp, J. P. Allebach, and G. T.-C. Chiu, "Extrinsic signatures embedding and detection in electrophotographic halftone images through laser intensity modulation," *Proceedings of the IS&T's NIP22: International Conference on Digital Printing Technologies*, Denver, CO, September 2006, pp. 432–435.
26. S. Suh, J. P. Allebach, G. T.-C. Chiu, and E. J. Delp, "Printer mechanism level data hiding for halftone documents," *Proceedings of the IS&T's NIP22: International Conference on Digital Printing Technologies*, Denver, CO, September 2006, pp. 436–440.
27. A. K. Mikkilineni, P.-J. Chiang, G. T.-C. Chiu, J. P. Allebach, and E. J. Delp, "Data hiding capacity and embedding techniques for printed text documents," *Proceedings of the IS&T's NIP22: International Conference on Digital Printing Technologies*, Denver, CO, September 2006, pp. 444–447.
28. E. M. Williams, *The Physics and Technology of Xerographic Processes*. New York, NY: Wiley, 1984.
29. D. Kacker, T. Camis, and J. P. Allebach, "Electrophotographic processes embedded in direct binary search," *IEEE Transactions on Image Processing*, vol. 11, pp. 234–257, 2002.
30. P.-J. Chiang, A. K. Mikkilineni, O. Arslan, R. M. Kumontoy, G. T.-C. Chiu, E. J. Delp, and J. P. Allebach, "Extrinsic signature embedding in text document using exposure modulation for information hiding and secure printing in electrophotography," *Proceedings of the IS&T's NIP21: International Conference on Digital Printing Technologies*, vol. 21, Baltimore, MD, October 2005, pp. 231–234.